42nd AIAA Aerospace Sciences Meeting and Exhibit
5 - 8 January 2004, Reno, Nevada

AIAA 2004-412

# Semi-Empirical Modeling of SLD Physics

William B. Wright * QSS Group, Inc.

Mark G. Potapczuk * NASA Glenn Research Center



## Abstract

The effects of supercooled large droplets (SLD) in icing have been an area of much interest in recent years. As part of this effort, the assumptions used for ice accretion software have been reviewed. A literature search was performed to determine advances from other areas of research that could be readily incorporated. Experimental data in the SLD regime was also analyzed. A semi-empirical computational model is then presented which incorporates first order physical effects of large droplet phenomena into icing software. This model has been added to the LEWICE software. Comparisons are then made to SLD experimental data that has been collected to date. Results will be presented for the comparison of water collection efficiency, ice shape and ice mass.

## Nomenclature

| | |
|---|---|
| $a_p$ | particle acceleration (m/s$^2$) |
| $A_p$ | cross-sectional area of particle (m$^2$) |
| D | drag force (kg*m/s$^2$) |
| $D_a$ | distance between particles (m) |
| $D_{le}$ | Airfoil leading edge diameter (m) |
| d | particle diameter (m) |
| f | drop frequency (Hz) |
| g | gravitational constant = 9.8 m/s$^2$ |
| h | film thickness (m) |
| L | lifting force (kg*m/s$^2$) |
| m | particle mass (kg) |
| s | surface wrap distance (m) |
| t | Time (s) |
| V | Velocity (m/s) |
| $V_x$ | x-component of velocity (m/s) |
| $V_y$ | y-component of velocity (m/s) |
| Vol | volume (m$^3$) |
| x | horizontal direction (m) |
| $x_p$ | x-location of water particle (m) |
| $\dot{x}$ | first derivative of x-location of water particle with respect to time (x-component of particle velocity) (m/s) |
| $\ddot{x}$ | second derivative of x-location of water particle with respect to time (x-component of particle acceleration) (m/s$^2$) |
| y | vertical direction (m) |
| $y_0$ | y-value of the starting locations of collection efficiency trajectories (m) |
| $y_p$ | y-location of water particle (m) |
| $\dot{y}$ | first derivative of y-location of water particle with respect to time (y-component of particle velocity) (m/s) |
| $\ddot{y}$ | second derivative of y-location of water particle with respect to time (y-component of particle acceleration) (m/s$^2$) |

### Dimensionless Numbers

| | |
|---|---|
| $c_l$ | coefficient of lift $= \dfrac{L}{A_p \rho_a V^2/2}$ |
| $c_d$ | coefficient of drag $= \dfrac{D}{A_p \rho_a V^2/2}$ |
| Eo | Eötvös number $= \dfrac{a_p \rho_w d^2}{\sigma}$ |
| f* | dimensionless drop frequency $= f\dfrac{d}{V}$ |
| Fr | Froude number $= \dfrac{V}{\sqrt{dg}}$ |
| K | Mundo splashing parameter $= Oh\,\mathrm{Re}^{5/4}$ |
| $K_{mt}$ | Marengo and Tropea parameter $= \dfrac{K^{8/5} f^{*\,6/5}}{10000}$ |
| La | Laplace number $= \dfrac{\rho_w \sigma d_o}{\mu^2}$ |
| Oh | Ohnesorge number $= \dfrac{\mu}{\sqrt{\rho\sigma d}}$ |
| Re | Reynolds number $= \dfrac{\rho V d}{\mu}$ |
| We | Weber number $= \dfrac{\rho V^2 d}{\sigma}$ |

* Senior Member, AIAA

### Greek Letters

| | |
|---|---|
| $\alpha$ | angle of attack (degrees) |
| $\beta$ | collection efficiency (dimensionless) |
| $\beta_0$ | angle difference between particle velocity vector and air flow velocity vector (radians) |
| $\delta$ | film thickness (dimensionless = h/d) |
| $\mu$ | viscosity (kg/ms) |
| $\nu$ | kinematic viscosity of air ($m^2/s$) |
| $\rho$ | density ($kg/m^3$) |
| $\sigma$ | surface tension ($kg/s^2$) |
| $\theta$ | impact angle (degrees) |
| $K_w$ | empirical splash parameter |

### Subscripts

| | |
|---|---|
| a | air |
| I | ice |
| n | normal direction |
| o | incoming drop value |
| p | particle |
| s | splashed drop value |
| t | tangential direction |
| w | water |
| x | x-dependent |
| y | y-dependent |
| $\infty$ | free-stream property |

## Introduction

In 1996, the authors presented a report[1] that assessed the capabilities of ice accretion software in the supercooled large droplet (SLD) regime. This effort was performed as a response to the 1994 crash of an ATR-72 in Roselawn, IN[2]. It has been speculated that accident occurred due to the accumulation of SLD ice aft of the deicing boots. Since then, several experimental efforts have been made to document SLD ice shapes and to investigate the underlying physics. This report will present modifications made to the ice accretion software, LEWICE[3], based upon observations from those tests.

The report is divided into three sections. The first section will provide a description of the LEWICE ice accretion model, with emphasis on particle trajectory and impact physics. It will include a review of related physics that have been studied in other research areas. The second section will describe the modified equations including analysis and observations from tests performed in the NASA icing research tunnel (IRT). The third section will provide comparisons of collection efficiency, ice shape and ice mass from those tests with the current model.

## LEWICE

The computer program, LEWICE, embodies an analytical ice accretion model that evaluates the thermodynamics of the freezing process that occurs when supercooled droplets impinge on a body. The atmospheric parameters of temperature, pressure, and velocity, and the meteorological parameters of liquid water content (LWC), droplet diameter, and relative humidity are specified and used to determine the shape of the ice accretion. The surface of the clean (un-iced) geometry is defined by segments joining a set of discrete body coordinates. The software consists of four major modules. They are 1) the flow field calculation, 2) the particle trajectory and impingement calculation, 3) the thermodynamic and ice growth calculation, and 4) the modification of the current geometry by addition of the ice growth.

LEWICE applies a time-stepping procedure to "grow" the ice accretion. Initially, the flow field and droplet impingement characteristics are determined for the clean geometry. The ice growth rate on each segment defining the surface is then determined by applying the thermodynamic model. When a time increment is specified, this growth rate can be transformed into an ice thickness and the body coordinates are adjusted to account for the accreted ice. This procedure is repeated, beginning with the calculation of the flow field about the iced geometry, then continued until the desired icing time has been reached.

Collection efficiencies are calculated in LEWICE through the use of a particle trajectory analysis. Droplets are released from a point in the freestream flow and tracked through the flow field using the following equations:

$$m\ddot{x}_p = -D\cos\beta - L\sin\beta + mg\sin\alpha$$

$$m\ddot{y}_p = -D\sin\beta + L\cos\beta - mg\cos\alpha$$

where

$$\beta = a\tan\frac{\dot{y}_p - V_y}{\dot{x}_p - V_x}$$

$$D = c_d \frac{\rho_a V^2}{2} A_p$$

$$L = c_l \frac{\rho_a V^2}{2} A_p$$

$$V = \sqrt{(\dot{x}_p - V_x)^2 + (\dot{y}_p - V_y)^2}$$

The initial release point in the x-direction is determined by finding an x-location where all of the velocities in a vertical sweep are within 0.1% of the freestream value. The initial release point in the y-direction is determined from the angle of attack. The initial velocity is assumed to be the terminal droplet velocity, which is given by

$$c_d \mathrm{Re}_t^2 = \frac{4gd(\rho_w - \rho_a)}{3\mu_a^2 \rho_a}$$

where

$$\mathrm{Re}_t = \frac{V_t d}{\mu_a}$$

Each droplet is then tracked until it either hits the airfoil or reaches the trailing edge. After the first trajectory ends, the next particle is released from a higher or lower starting point in an attempt to hit the surface. This process is continued until there exists at least one drop that passes above the airfoil and one that passes below.

Impingement limits are then found using a standard bisection search algorithm. Using the coarse limits found in the prior step, LEWICE starts a drop halfway between these limits. Based upon the end result of that trajectory, the next drop is released halfway between the current starting point and the starting point of either the upper or lower coarse limit. The coarse limit is then refined based upon the trajectory results. This process is repeated until the starting point of a drop that hits the airfoil and the starting location of a drop that misses the airfoil is within $10^{-5}$. The bisection is then repeated to find the second impingement limit.

Collection efficiency is then determined by sending a user-determined number of trajectories uniformly spaced between the impingement limit starting locations. The starting and ending locations of these trajectories is stored. Collection efficiency is then calculated by the following definition:

$$\beta \equiv \frac{dy_o}{ds}$$

## Literature review

This section will present various assumptions used in the collection efficiency calculation in LEWICE. While other surface physics such as evaporation, rivulet flow and film dynamics are important to the water impact, much of this review centers on trajectory and splashing phenomena. The review will focus on effects for larger droplets. A large drop in this context applies to any drop size larger than 40 μm, the current upper limit in the FAA certification envelope. LEWICE uses the following assumptions in the trajectory equations:

- solid particles
- spherical particles
- drops do not break up
- particles do not rotate
- particles have no lift
- particles have no moment
- drag for a stationary sphere applies
- no transient effects of drag
- evaporation of the drop is negligible
- turbulence effects are neglected
- flow is incompressible
- gravity is considered
- drops do not interact with each other
- continuum flow around drop
- all drops that strike the airfoil impinge

Droplet motion and impact has a wide variety of applications and has been studied extensively in several research areas. Much of the early work was summarized by Clift, Grace and Weber[4] and also by Tavlarides et. al.[5]. A summary of more recent research was performed by Michaelides[6].

### Third Order Effects

Third order effects in this context refers to physical effects that are negligibly small. Therefore this section will review physical effects that can safely be ignored in the SLD regime. First, the Basset force models the effect of the change in drag as a function of time. This term is also called the drag history term. It is used to model the flow of gas bubbles, particularly when they are immersed in air. This effect is unimportant for cases where the viscosity of the surrounding fluid is less than the

particle viscosity. Since the viscosity of air is much less than that of water, this term is safely ignored.

A lift force for small particles was described by Saffman[7]. The Saffman force is often described as a "champagne bubble" effect and is more important for gas bubbles than for liquid particles. It is also more important for very small particles (smaller than the 15$\mu$m Appendix C limit) than for the larger particles that are being studied. Saffman and Basset forces have been calculated in LEWICE and both were found to be extremely negligible.

Turbulence effects have been studied by several authors. The works of Mashayek[8], Marchioli and Soldati[9], and Shin et. al.[10] perform DNS calculations of turbulence effects on particles, including effects near a solid boundary. All of these studies are limited to particle sizes much smaller than 15$\mu$m. Particles in the Appendix C and SLD matrices are less susceptible to turbulence effects. The small effect of turbulence in SLD can be seen in the IRT and other icing tunnels. Tunnel uniformity depends partly on the droplets being dispersed due to turbulence. Some of the difficulty in achieving tunnel uniformity can be attribute to this factor. Turbulent effects effects have been studiedby Bhargava, et al[11] in their simulation of water droplet clouds in the IRT. Compressibility effects are considered unimportant unless higher speeds, such as those that occur with rotor blades or propellers, are encountered.

### *Gravitational Effects*

LEWICE models gravity both as a force during the trajectory calculation and by using the drop's terminal velocity as an initial condition for the drop. As drop size increases, the gravitational force will become more significant both in terms of this initial velocity vector and in the subsequent trajectory path. However, even at extremely large drop sizes, gravity has a third order effect on collection efficiency.

This effect was illustrated in the following test case. An icing simulation was performed for an MS317 airfoil with LEWICE using a 10-bin, 236$\mu$m MVD. This drop size distribution has the largest MVD of the impingement database[12]. The case was computed including gravitational force and then repeated with that force turned off in LEWICE. This simulates the difference in collection efficiency that would occur between a wing that is mounted horizontally in a tunnel with one that is mounted vertically. As seen in this figure, gravity has a negligible effect on water collection. The only gravitational differences in LEWICE are at the impingement limits. However, comparisons with experiments have shown that LEWICE overestimates water collection at the impingement limits, thus the effect of gravity may be even less than shown here.

**Figure 1: Effect of Gravity on Collection Efficiency**

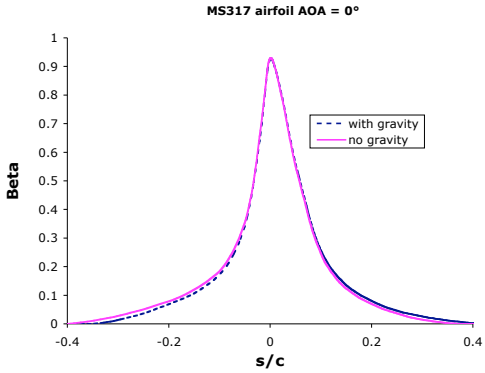


Another way to look at the effect of gravity is the Froude number. The Froude number is the ratio of inertia force to gravitational force and is given by:

$$Fr = \frac{V}{\sqrt{dg}}$$

The following plot shows the range of Froude numbers that can occur in icing. This plot shows that even at extremely high drop sizes, the Froude number is close to 1000. A Froude number of 1000 means that inertia forces are still 1000 time more important than gravitational forces.

**Figure 2: Froude Number Range in Icing Analysis**

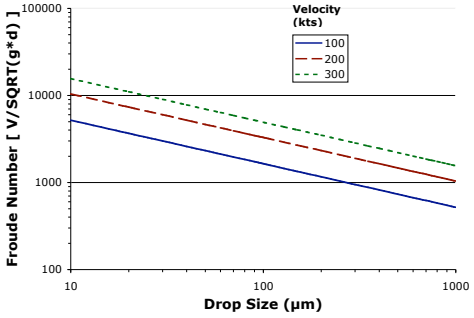

## Second Order Effects

Second order effects in this context refers to physical effects that can have a minor affect on water collection under certain conditions. These effects are modeled by LEWICE but have been found to be small when compared to the inertia force and to the surface dynamics of splashing.

### *Solid and Spherical Particles*

This assumption states that the drop remains spherical and does not deform due to the drop velocity. It also assumes that there is no internal flow within the drop. The literature reviews cited earlier demonstrate that the preferred method of accounting for a change in drop shape or internal flow in a drop is to change the drag and lift using empirical equations. Beard and Pruppacher[13] measured large raindrops falling in air at terminal velocity due to gravity and showed that the non-spherical shape can be accounted for by using an alternate drag model, which at most is 15% higher than the drag on a sphere. This drag model is shown in Figure 3. In addition, their tests showed negligible effect on lift and moment.

**Figure 3: Drag Increase Due to Non-spherical Particles**

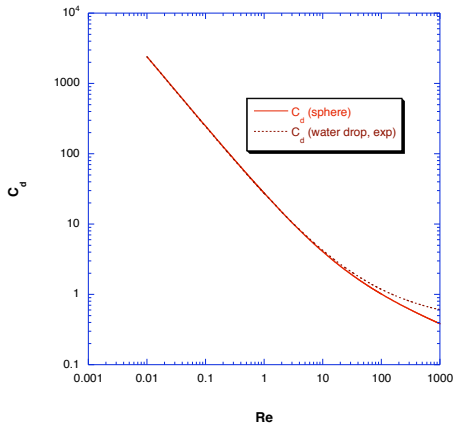


A test case was then constructed using an MS-317 airfoil. The following conditions were used:

□ = 2°
LWC= 0.34 g/m$^3$
V= 195 mph
T= -10°C
MVD=1000 $\mu$m
□

The first case uses the standard drag model used in LEWICE. This drag model uses a correlation of the experimental drag values in Figure 1. The second case then increased this value 15% for the entire Reynolds number range. This is a more severe requirement than the Beard and Pruppacher model where the drag at low Reynolds numbers conforms to the standard model. In addition, this case only accounts for the drag increase due to deformation and does not consider breakup. The actual drag increase will be less due to the drop breakup. The collection efficiencies for these two cases are shown in Figure 4. As can be seen from this figure, the effect of drop deformation on collection efficiency is negligible.

**Figure 4: Drag Effect of Non-spherical Drop**

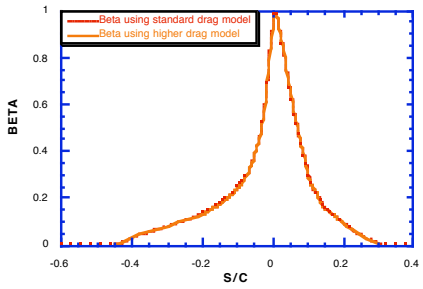


### *Drop Interaction*

LEWICE assumes that the particle stream is sparse enough that interaction effects (such as droplet collisions) do not exist or are rare enough to be neglected. This assumption allows the solution of each drop size in the distribution separately. This assumption also neglects the effect of particle density on the airflow solution, allowing the airflow to be determined a priori (uncoupled). Mulholland et. al.[14] studied the effect of droplet spacing and showed that for droplet Reynolds numbers less than 250, local particle densities greater than 0.3 g/m$^3$ could cause a decrease in drag coefficient. However, even for particle densities of 3 g/m$^3$, the effect on droplet drag was less than 5%.

A second factor that has not been studied extensively concerns droplet interactions near the wall during a splash event. Smyrnaios et. al.[15] studied the effect of heavy rain on airfoils and predicted premature boundary layer separation for an LWC of approximately 3 g/m$^3$ using a Direct Numerical Simulation (DNS) model. A splashing event can result in a high density of

particles near the wall that may interact with the incoming droplets. The effects on the boundary layer and the trajectories of incoming particles may be taken into account by methods that use particle density (by means of droplet frequency) in their splashing models. This effect will be discussed in the review of splashing effects.

*Drop Breakup*

If a large drop moves at a high enough velocity, it can breakup due to shear. Breakup occurs when the drop passes a critical Weber number. Values for this critical Weber number vary widely in the literature.

The Weber number is given by:

$$We_p = \frac{\rho_a V^2 d}{\sigma}$$

For water drops falling at their terminal velocity, the critical Weber number (based on air density) is approximately 10. For water drops accelerated by a shock wave, a value of 6.5 is given. Krzeczkowski[16] and Hsiang[17] each measured droplet breakup for shear induced flows and reported values ranging from 10 to 20. Ibrahim et. al.[18] provided a more detailed analysis of the droplet deformation and breakup using a Taylor analogy model. The Weber number of each trajectory was output from LEWICE for the case described above to investigate this effect. A contour plot of Weber number is shown in Figure 5 and shows that the Weber number clearly indicates that drop breakup occurs for this drop size.

**Figure 5: Weber Number on 1000 Micron Drop**

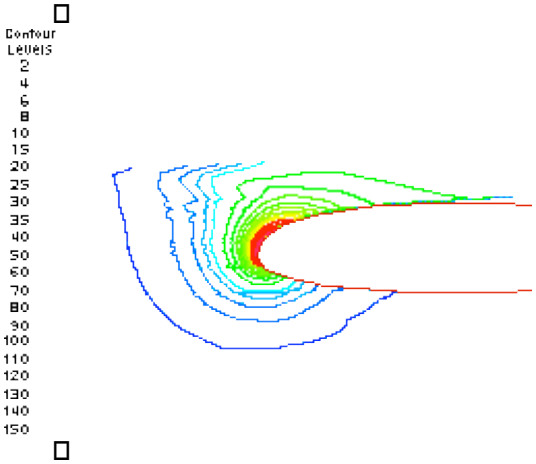


Drop breakup is also attributed to the Eötvös number, which is given by

$$Eo_p = \frac{a_p \rho_w d^2}{\sigma}$$

where

$$a_p = \sqrt{\ddot{x}^2 + \ddot{y}^2}$$

is the acceleration of the particle.

A critical Eötvös value of 16 or higher is cited for drop breakup. The corresponding plot of Eötvös number is shown in Figure 6. This shows that although the Weber number is high enough to cause breakup, Eötvös number is not. The remaining analysis there fore only considers breakup due to the Weber number criteria.

**Figure 6: Eötvös number on 1000 micron drop**

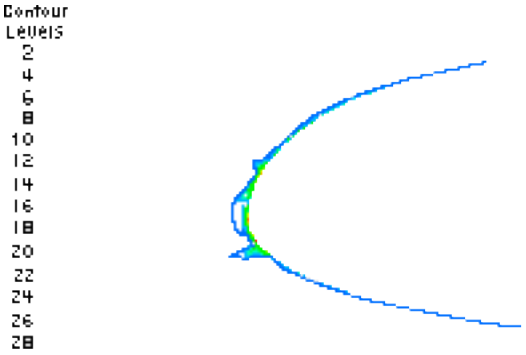


The case for a 1000$\mu$m drop clearly shows that according to the Weber number criteria, drops will breakup before reaching the airfoil. At this point, it is unclear how this breakup affects the collection efficiency. The smaller drops produced will tend to be deflected more, however by the time they reach critical Weber number values, they are only 0.1 chord from the leading edge even in this extreme example. As most of the particle deflection occurs within this region and since drops tend to break up into much smaller drops, it seems feasible that there is some mass loss that can be attributed to this factor.

An empirical relationship found in Hsiang and Faeth[17] was added to LEWICE in order to estimate the reduction of collection efficiency due to breakup. In their model, droplets will start to break up when the critical Weber number is greater than 13. This Weber number is based on the air density as defined earlier in this report. Since droplet breakup occurs rapidly compared to the trajectory time step, breakup is considered to be instantaneous. Dai and Faeth[19] produced

some excellent photographs of the breakup process using pulsed shadowgraphy and holography.

Secondary particle size is given by the following equation:

$$d_n = 6.2\left(\frac{\rho_w}{\rho_a}\right)^{1/4} \mathrm{Re}_w^{1/2} d_o$$

where

$$\mathrm{Re}_w = \frac{\rho_w V d}{\mu_w}$$

This correlation can be applied to an Eulerian system as well as the Lagrangian tracking system used by LEWICE. However, it would be necessary in a Eulerian system to solve coupled sets of equations for each drop size generated. In the Lagrangian system, the smaller drop size is simply tracked from the breakup location. An empirical relationship was chosen to assess the importance of breakup to the collection efficiency. If breakup is not important then there is no need to implement the more complicated droplet deformation and breakup (DDB) model described by Ibrahim[18].

The MVD=236$\mu$m case shown earlier for the MS317 airfoil was the first case chosen to illustrate the effect of breakup. Figure 7 shows the case with and without breakup. An analysis of the droplet trajectories shows that breakup does occur in this case.

**Figure 7: Effect of Droplet Breakup on Collection Efficiency**

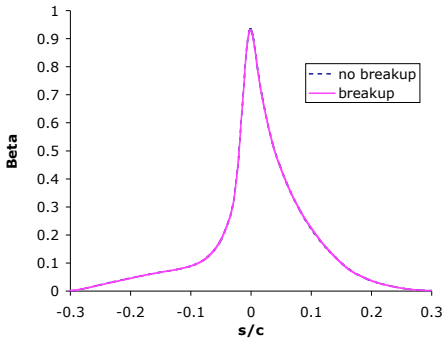


To further illustrate the potential effect of breakup, a second example was chosen. In this case, a three section multi-element airfoil shown in Fig. 8 was chosen since breakup will occur only in regions of high velocity gradient. The conditions for this case were chosen to represent the most extreme environment possible.

**Figure 8: Multi-Element Airfoil Used for Drop Breakup Analysis**

For this case, the chord length (stowed) was 3.96 m, the angle of attack was 8° and the MVD was 560$\mu$m with a 7-bin distribution. The droplet distribution was taken from a draft of the Appendix X conditions[20]. In this case, droplet breakup does affect the collection efficiency, especially for the slat. This result is expected since droplets near the leading edge of a slat will exhibit the highest shear velocities.

**Figure 9: Breakup Effect on Slat**

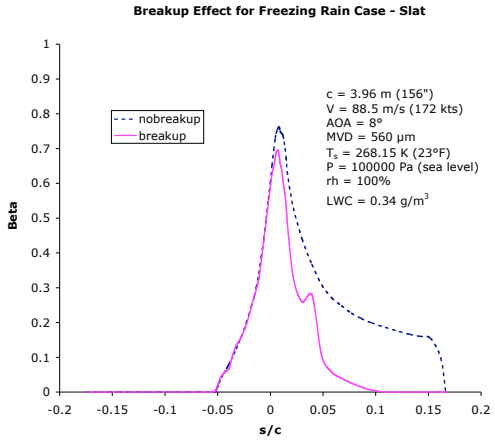


**Figure 10: Breakup Effect on Main Element**

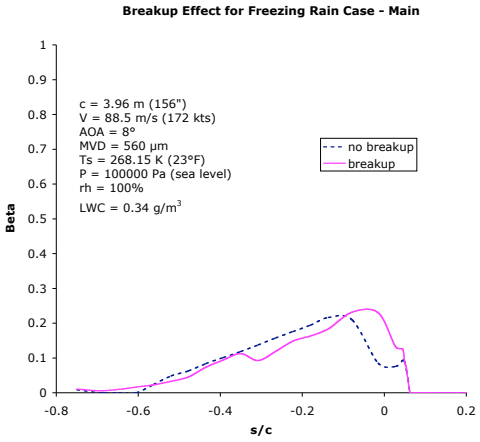


**Figure 11: Breakup Effect on Flap**

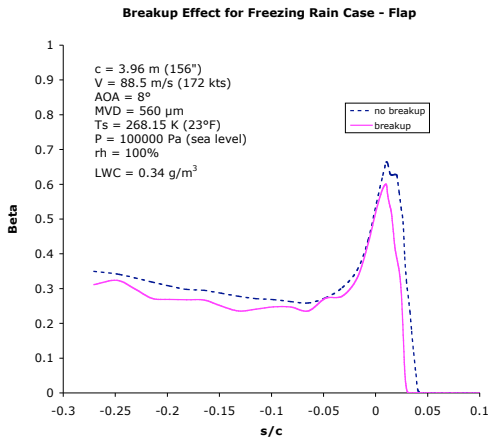


### *Ice Density*

In the past, LEWICE has always been compared to experimental data through the comparison of the ice shape profile. These comparisons only use the ice shape geometry and not the ice mass. Recently, Potapczuk[19] measured both ice shape and ice mass on a NACA0012 airfoil in the IRT. It was shown that ice mass decreased as a function of drop size which suggests a mass loss due to splashing. However, even though mass decreased, many ice shape profiles did not. This result demonstrated that the ice density was also decreasing with increasing drop size. While the ice mass data accumulated so far is insufficient for generating an accurate correlation, the following expression was used for the ice shape comparisons in this report:

$$\rho_i = 920 - 2 * d_o$$

## First Order Effect: Drop Splashing

The literature search performed for this report confirms that the primary assumption LEWICE uses that is invalidated for SLD is the assumption that all drops that strike the surface impinge, thus neglecting splashing and/or bouncing of drops. One of the earliest detailed experimental studies was performed by Stow and Hadfield[22] who reported on the impact of water drops on a dry surface. Macklin and Metaxas[23] reported a similar study that also used ethanol and glycerol to study the effect of different fluid properties. Jayarante and Mason[24] looked at bouncing and splashing of raindrops impinging at various angles on dry surfaces and films. Wright[25] developed a theoretical splash model for raindrops for the purpose of modeling soil erosion.

Harlow and Shannon[26] solved the Naviér-Stokes equations for the impact of a single drop on a dry surface or film. A more recent work was performed by Yarin and Weiss[27,28] who proposed a splashing model as a type of kinematic discontinuity. Other works include Rein[29] who provides a review of several papers, including phenomena such as bouncing along with splashing and coalescence and Chandra and Avedisian[30] who documented photographically the droplet structure during the deformation process.

Computationally, a detailed physical model of droplet splashing would require solving the Naviér-Stokes equations for each droplet impact using a Volume of Fluid (VOF) model such as that described by Hirt[31]. Examples of this type of calculation were reported by Trapeaga and Szekely[32] as well as Tan and Papadakis[33]. Current computational capabilities usually limit this approach to single drop calculations. In a typical icing encounter, thousands of droplet impacts are recorded per second, making this type of analysis prohibitively expensive. An empirical or semi-empirical approach is therefore necessary.

A recent experimental study by Mundo, Sommerfeld and Tropea[34-6] examined droplet-wall collisions and correlates splashing in terms of Reynolds number and Ohnesorge number

$$Oh = \frac{\sqrt{We}}{\mathrm{Re}} = \frac{\mu}{\sqrt{\rho \sigma d}}$$

The Reynolds and Ohnesorge numbers are based on the liquid properties and the component of the impact velocity normal to the surface. Based on the results of their experiment, splashing occurs if the factor $K=Oh*Re^{1.25}$ is greater than 57.7. A plot of this parameter for drop sizes of 20 and 200 microns is shown in Figure 12.

**Figure 12: K-factor for droplet splash**

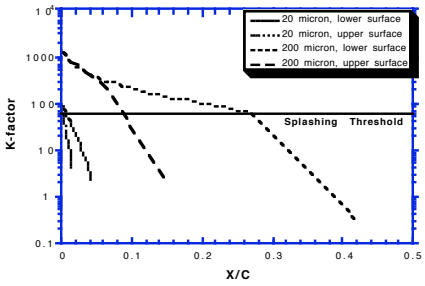


A small amount of droplet splash is seen in Fig. 5 even for a 20 micron drop, showing that this phenomena will occur at much lower drop sizes than droplet break up. This figure also shows that droplet splashing is a significant factor in the large drop regime.

The Mundo papers also provide a characterization of the size, velocity and direction of the splashed particles. Their later references provide an empirical splashing model that can be used in Lagrangian tracking schemes. The empirical formulas calculate splashed drop size, splash velocity, splash angle and deposited mass as functions of the incoming parameters. The Mundo expressions are given below.

$$K = \left( \frac{\rho_w^3 d^3 V_n^5}{\sigma^2 \rho_w} \right)^{1/4} \geq 57.7 \text{ for splash}$$

$$\frac{d_s}{d_o} = 8.72 e^{-0.0281K}; \; 0.05 \leq \frac{d_s}{d_o} \leq 1$$

$$n_s = 1.676 * 10^{-5} K^{2.539}; \; n_s \leq 1000$$

$$\frac{V_{t,s}}{V_{t,o}} = 1.337 - 1.318 \frac{d_s}{d_o} + 2.339 \left( \frac{d_s}{d_o} \right)^2$$

$$\frac{V_{n,s}}{V_{n.o}} = -0.249 - 2.959 \frac{d_s}{d_o} + 7.794 \left( \frac{d_s}{d_o} \right)^2$$

$$\frac{m_s}{m_o} = n_s \left( \frac{d_s}{d_o} \right)^3$$

Some observations can be derived from these expressions. First, for K<77, drops bounce (size out = size in). At the splashing onset, roughly half will bounce, since half the mass is lost and the size of the drops has not changed. At K=77, all of the drops will bounce, as the outbound size has not changed and the mass loss is 100%. According to this model, the breakup of a drop into smaller particles doesn't really occur until K>77. Splash mass is 0.15% at his upper K limit and shows asymptotic behavior. Finally, these correlations are only valid up to a drop size of 150$\mu$m and a drop speed of 18 m/s. This range is much lower than that needed for icing analysis.

However, there are additional problems with this approach. If we assume that the splashing measured by Mundo scales into the icing regime (higher velocity and initial drop size), then maximum mass loss (K=77) would be greatest in Appendix C regime, not SLD. Additionally, the correlations given above do not make physical sense. For example, this report gives 1000 as the maximum number of drops that can be generated from a single splash. However, the correlation gives only nine drops generated at K=180, the upper limit of his data. Mundo also gives droplet velocity correlations that do not conserve momentum at the lower range of his K-values.

Based on these discrepancies, additional reports were sought to determine correlations more suited for use in icing. Several authors provided empirical models for the splashing threshold or for splashed drop size. However, a complete model including splashed mass loss and splashed velocity was sought so that it could be implemented into LEWICE. The following section provides a summary of the splashing models found to date.

### *Summary of Splashing Models*

The parameters needed for an empirical splashing model are the splashing threshold, the splashed drop size (or drop size distribution), the splashed velocity (or a distribution of splash velocities), the splash angle (or a distribution of splash angles) and the amount of splashed mass. The number of splashed particles is needed only if all splashed particles are to be tracked. The models presented typically provide these variables as a ratio to the incoming parameters. Some of the older and less developed splashing models found in the literature were not included in this summary.

Many of these models include the effects of droplet frequency, f, and the dimensionless film thickness d. As stated earlier, splashed droplets are likely to interact with incoming drops. Since this physical effect occurs in the experiments reviewed below, it was assumed unnecessary to otherwise account for droplet-droplet

interactions. Droplet frequency can be calculated from the liquid water content by assuming that particles are uniformly distributed in the freestream. The drop frequency is defined as the mass flow rate of water divided by the particle mass. The volume of air around each drop is assumed spherical with a circular cross-section. Therefore,

$$f = \frac{\dot{m}}{m} = \frac{LWC * V * \frac{\pi}{4} D_a^2}{\rho_w * \frac{\pi}{6} d^3} = \frac{3}{2} \frac{LWC}{\rho_w} \frac{V}{d} \left( \frac{D_a}{d} \right)^2$$

However, liquid water content (LWC) is the mass of water per volume air, thus:

$$LWC = \frac{\rho_w \frac{\pi}{6} d^3}{\frac{\pi}{6} D_a^3} = \rho_w \left( \frac{d}{D_a} \right)^3$$

Eliminating $D_a$ yields the following expression for drop frequency:

$$f = \frac{3}{2} \frac{V}{d} \left( \frac{LWC}{\rho_w} \right)^{1/3}$$

The correlations implemented into LEWICE calculate frequency from the MVD and the overall LWC. If necessary, it could also be calculated from the individual droplet spectrum. Film thickness was estimated from a correlation provided by Feo[37]:

$$\delta = 3.76 \left( \frac{D_{le}}{d} \right)^{5/4} \left( \frac{LWC}{\rho_w} \right)^{1/2} We_{le}^{-1/8}$$

The correlations provided in this report were developed using similar experimental techniques and therefore had similar ranges of applicability. The upper limit on drop size and velocity were 340$\mu$m and 30 m/s respectively. Droplet frequency and film thicknesses were in the range expected for icing encounters except at the lower range. Splash data exists for dry surfaces ($\delta$=0) and for film thicknesses of $0.3<\delta<3$. The applicability of these models to very thin films is unknown. Similarly, droplet frequencies are lower in the SLD range due to the lower water contents as well as the higher drop sizes. However, the correlations are well behaved in these limits and tend toward limiting values.

*Lee and Ryou Model*

Lee and Ryou[38] proposed the following statistical model:

$$\frac{V_{t,s}}{V_{t,o}} = 5/7$$

$$\frac{V_{n,s}}{V_{n,o}} = -0.993 + 1.76\delta_o - 1.56\delta_o^2 + 0.49\delta_o^3$$

$$\frac{m_s}{m_o} = 0.2 + 0.9RN(0,1)$$

$$n_s = 0.187We_o - 4.45$$

$$\frac{d_s}{d_o} = \left( \frac{m_s}{m_o} \frac{1}{n_s} \right)^{1/3}$$

where RN(0,1) is a random number between 0 and 1. This approach requires a large number of trajectories to be calculated in order to achieve a statistical sampling. This occurs because the splashed mass and splashed drop size are calculated using a random number. The underlying assumption is that the phenomena is chaotic.

*Stanton and Rutland Model*

Cossali et. al.[39] summarized a number of splashing models and made comparisons to their data. One of these models was derived by Stanton and Rutland[40] using a complex correlation from the data of Yarin and Weiss[28]. They used a distribution of splashed droplets rather than a single splashed drop in their model. This approach would also require calculation of a large number of splashed droplet trajectories since each incoming drop would produce a distribution of splashed particles. The correlation is given by the following equations:

$$K_c = 324\left(f^*\right)^{3/4}$$

$$f^* = f\frac{d}{V} = \frac{3}{2}\left(\frac{LWC}{\rho_w}\right)^{1/3}$$

$$pdf\left(\frac{d_s}{d_o}\right) = \left(\frac{b}{\sigma_w}\right)\left(\frac{d_s/d_o}{\sigma_w}\right)^{b-1}\exp\left[-\left(\frac{d_s/d_o}{\sigma_w}\right)^{b}\right]$$

where

$$b = 2.71 - 9.25*10^{-4}We$$

$$\sigma_w = 0.21 - 7.69*10^{-5}We$$

$$pdf\left(\frac{V_{n,s}}{V_{n,o}}\right) = \left(\frac{b_v}{\sigma_v}\right)\left(\frac{V_{n,s}/V_{n,o}}{\sigma_o}\right)^{b_v-1}\exp\left[-\left(\frac{V_{n,s}/V_{n,o}}{\sigma_v}\right)^{b_v}\right]$$

where

$b_v = 2.1$ for $\theta_i \le 50°$

$b_v = 1.1 + 0.02\theta_i$ for $\theta_i > 50°$

$$\sigma_v = 0.158e^{0.017\theta_o}$$

$\theta_s = 65.4 + 0.266\,\theta_o$

$V_t = V_n \cot \theta_s$

### *Marengo and Tropea Model*

Marengo and Tropea[41] used a similar form for drop size and velocity components:

$$\frac{d_s}{d_o} = (0.25 + 0.238\theta)\left(0.22 + 1.28\theta\right)\left(K_{mt} - K_{mt,c}\right)$$

$$K_{mt} = K^{8/5}f^{*6/5}*10^{-5}$$

$$\frac{V_{t,s}}{V_{t,o}} = \left(0.056 + 0.057\theta\right) + 0.38\left(K_{mt} - K_{mt,c}\right)$$

$$\frac{V_{n,s}}{V_{n,o}} = \left(0.311 - 0.077\theta\right)\left(0.09 + 0.24\theta\right)\left(K_{mt} - K_{mt,c}\right)$$

$$\frac{m_s}{m_o} = \left(0.363 + 0.242\theta\right)\left(K_{mt} - K_{mt,c}\right)^{2.928-1.521\theta}$$

$$n_s = 641.8 + \frac{640.8\left(K_{mt} - K_{mt,c}\right)}{1 + e^{\left(K_{mt} - K_{mt,c}\right)}}2^{(0.675+0.036\theta)\left(K_{mt} - K_{mt,c}\right)}$$

### *Trujillo Model*

Trujillo et. al.[42] used Mundo's drop size expression but used different forms for the other variables. Their correlation can be expressed by:

$$\frac{V_{n,s}}{V_{n,o}} = 0.85 + 0.0025\theta_o$$

$$\frac{V_{t,s}}{V_{t,o}} = 0.12 + 0.002\theta_o$$

$$\frac{m_s}{m_o} = 0.2\left[1 - \exp\left(-K^{1/2}f^{*3/8}K_c^{1/2}f_c^{*3/8}\right)\right]$$

$$n_s = \frac{1}{22}\left[0.0437K\left(\frac{V_{x,o}}{V_{y,o}}\right)^2 K_c - 44.92\right]$$

### *Schmehl Model*

Schmehl et. al.[43] assumed that the splash velocity was 60% of the incoming velocity and used the following expressions for the remaining terms:

$$\ln\frac{d_s}{d_o} = -2 - \frac{d_o}{4066} - 0.05S$$

$$S = \frac{\mathrm{Re}}{24La^{0.419}};\ La = \frac{\rho_w\sigma d_o}{\mu^2} = \frac{1}{Oh^2}$$

$$\left(\frac{m_s}{m_o}\right)_{dry} = 1 - S^{-3/5}$$

$$\left(\frac{m_s}{m_o}\right)_{film} = \left(\frac{m_s}{m_o}\right)_{dry} e^{\square\square}$$

*Samenfink Model*

Finally, Samenfink et. al.[44] used the following expressions:

$$\frac{d_s}{d_o} = 1 \square 0.03454 S^{0.175} \square_o^{0.1239} La^{0.265}$$

$$\frac{V_s}{V_o} = 0.08214 S^{\square 0.3384} \square_i^{0.2938} \square^{0.03113} La^{0.1157}$$

$$\square_s = 2.154 S^{1.0946} \square^{0.03389} \square^{\square 0.1589}$$

$$V_{n,s} = V_s \sin\left[\frac{\square\square_s}{180}\right]; \; V_{t,s} = V_s \cos\left[\frac{\square\square_s}{180}\right]$$

$$\frac{m_s}{m_o} = 0.0866\left(S \square 1\right)^{0.3188} \square_o^{0.1223} \square^{0.9585}$$

In this model, the splashing parameter S has the same definition as used in the Schmehl model and splashing occurs for S > 1.

## Collection efficiency results

By knowing the splashing parameters, a feature can be added to LEWICE to track the trajectories of the splashed particles and the trajectories of particles after breakup. This process was described in a recent report by Rutkowski, et. al.[45]. Mass loss due to splashing and subsequent reimpingement are also calculated. Since it is necessary to extrapolate from the experimental data for icing encounters, care must be taken, especially in high velocity impacts. The Trujillo model and the Samenfink model were programmed into LEWICE to assess the effects of splashing on water collection and ice accretion. These two models were chosen as the correlations tended to exhibit asymptotic behavior at higher velocities.

The MS-317 airfoil was chosen to demonstrate the effect of these splashing models on water collection. The MS-317 airfoil has been used in several IRT entries for measuring collection efficiency[12,46]. The conditions chosen were 0° and 8° angle of attack, and drop sizes of 21$\mu$m, 92$\mu$m and 236$\mu$m. The 21$\mu$m cases were chosen to show that although the models predict splashing in Appendix C conditions, very little mass is lost. The tunnel speed for all cases was 175 mph (152 kts, 78 m/s).

As can be seen in Figures 13 and 14, the collection efficiencies are very similar for the splashing and non-splashing cases. Slightly more water is lost using the Trujillo model than the Samenfink model, but the two results are comparable.

**Figure 13: Collection Efficiency for MVD = 21$\mu$m and AOA = 0°**

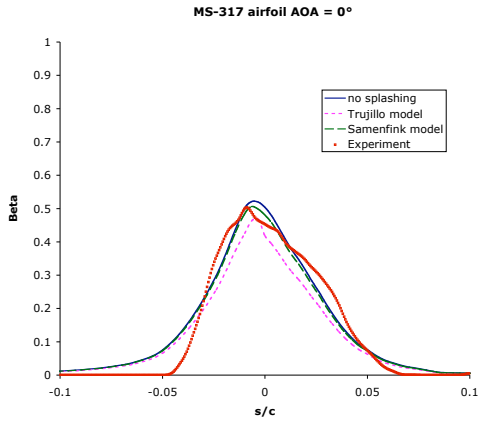


**Figure 14: Collection Efficiency for MVD = 21$\mu$m and AOA = 8°**

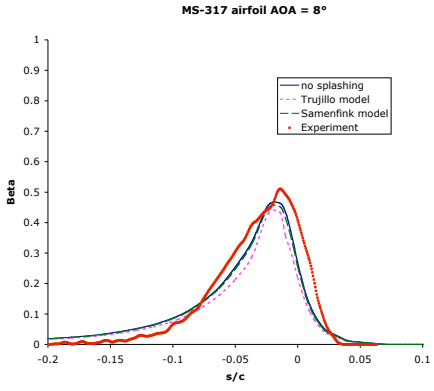


More mass loss is predicted for the 92$\mu$m cases shown in Figures 15 and 16. The models predict the mass loss at the leading edge very well, but do not capture the mass loss at the

impingement limits. This result is to be expected from the empirical models since the splashing parameters K and S are calculated using the normal component of the impact velocity.

**Figure 15: Collection Efficiency for MVD = 92$\mu$m and AOA = 0°**

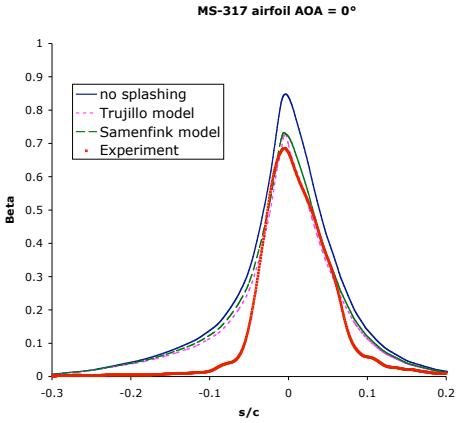


**Figure 16: Collection Efficiency for MVD = 92$\mu$m and AOA = 8°**

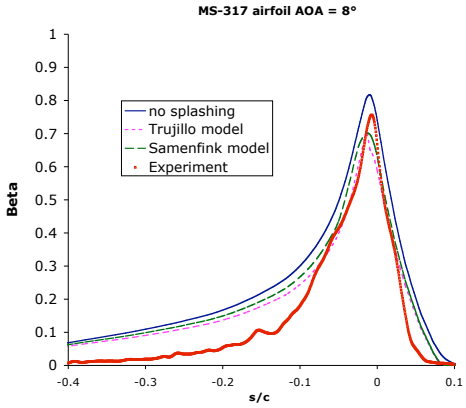


Figure 17 shows a plot of the impact velocity and the impact velocity components for a 241$\mu$m drop. The 241$\mu$m drop size was the largest drop used in the 92$\mu$m distribution. The impact velocity is almost the same at each chordwise location. This occurs because the drop size is so large its trajectory is almost ballistic. The normal component of the velocity is largest at the leading edge and decreases chordwise. Splashing will therefore have the largest effect at the leading edge according to these models. However, the splashing parameters in this regime are much greater than the upper limits of the experimental data. This suggests that while impingement near the leading edge may still be modeled using these equations, a new model is needed at the impingement limits.

**Figure 17: Impact velocity for a 241$\mu$m Drop**

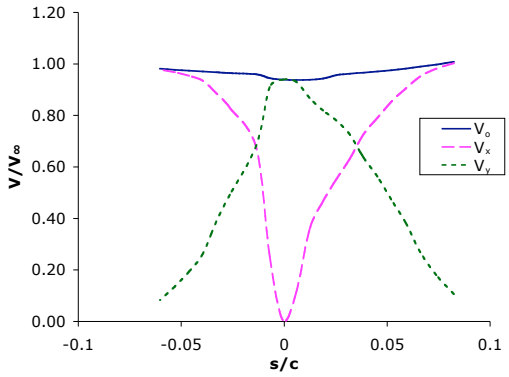


Figures 18 and 19 show the collection efficiency results for the 236$\mu$m case. This case represents the largest drop size for which collection efficiency data exists. The Trujillo model exhibits a similar behavior at 236$\mu$m as it did for the 92$\mu$m case, demonstrating that this model can be extrapolated somewhat from the experimental limits. The Samenfink model continues to show much higher mass loss at the higher drop size. This result is not considered realistic.

**Figure 18: Collection Efficiency for MVD = 236$\mu$m and AOA = 0°**

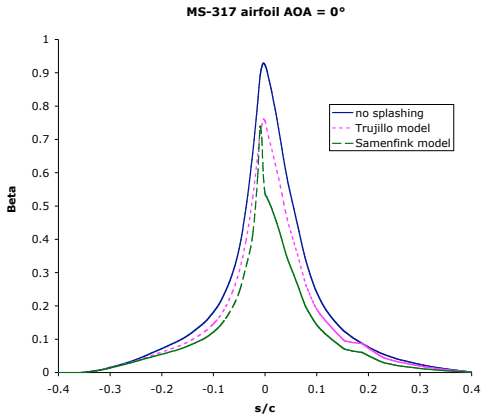

**Figure 19: Collection Efficiency for MVD = 236$\mu$m and AOA = 8°**

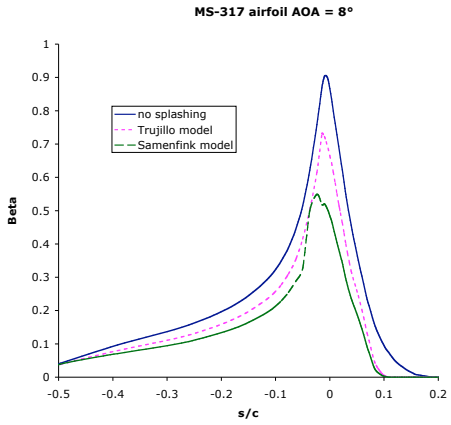


## Ice shape and mass results

The Trujillo model was then used along with the ice density correlation to generate ice shapes on a NACA0012 airfoil. The dataset chosen was reported on last year by Potapczuk[21]. This data was chosen as it also contained measurements of ice mass as well as ice shape. The conditions are shown in the following table.

**Table 2: Inputs for Ice Shape Cases**

| Case | MVD ($\mu$m) | LWC (g/m$^3$) | V (m/s) | $T_{tot}$ (°C) | time (sec) |
|---|---|---|---|---|---|
| Run 1-17 | 40 | 1.02 | 77 | -19.3 | 588 |
| Run 1-1 | 70 | 0.91 | 51 | -19.6 | 804 |
| Run 1-4 | 160 | 1.5 | 52 | -19.5 | 300 |
| Run 1-22 | 40 | 1.02 | 77 | -19.3 | 576 |
| Run 1-23 | 70 | 0.65 | 77 | -19.2 | 714 |
| Run 1-26 | 160 | 1.04 | 77 | -19.2 | 336 |

The first case shows the comparison for Run 1-17 and Run 1-22, the two 40$\mu$m drop size cases. The two conditions are very nearly identical and show a similar result. The comparison shows a slight decrease in the overall shape. Additionally, the shape is closer to a rime shape like the experiment. It should be noted that LEWICE 3.0 will generate the same ice shape as LEWICE 2.0 if the splashing model is deactivated.

**Figure 20: Ice Shape Comparison for Run 1-17**

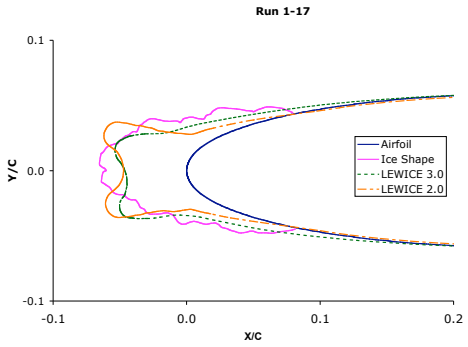


**Figure 21: Ice Shape Comparison for Run 1-22**

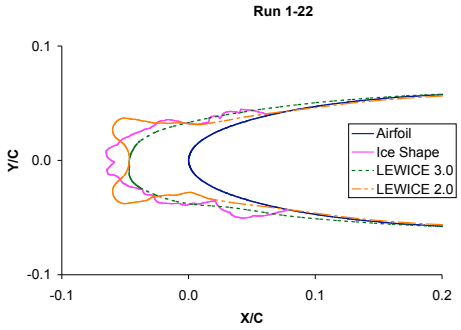


Figures 22 and 23 show the results for the 70$\mu$m cases. The conditions are scaled to produce the same accumulation parameter. These cases show very little difference between LEWICE 3.0 and the previous model. The mass loss due to splashing is nearly equal to the reduction in ice density, resulting in a similar shape.

**Figure 22: Ice Shape Comparison for Run 1-1**

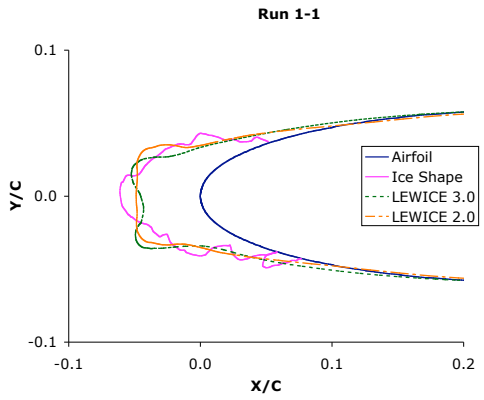


**Figure 23: Ice Shape Comparison for Run 1-23**

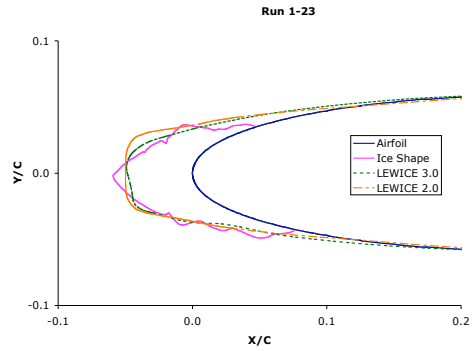


Figures 24 and 25 show the ice shape comparisons for the 160$\mu$m cases. Both cases produce a smaller and more streamlined shape than LEWICE 2.0 produced without splashing. The effect is more pronounced for Run 1-26 because the higher velocity will produce more splashing and hence mass loss.

**Figure 24: Ice Shape Comparison for Run 1-4**

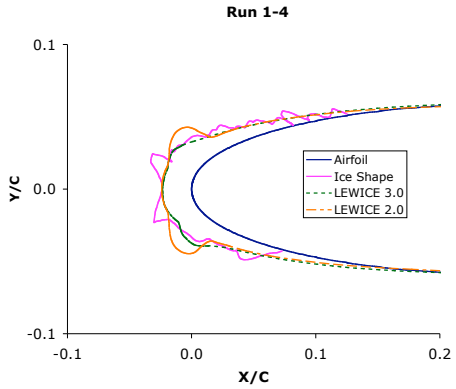


**Figure 25: Ice Shape Comparison for Run 1-26**

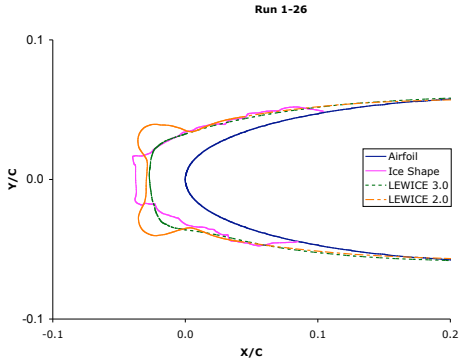


Finally, Figure 26 shows the prediction of ice mass for these conditions. The mass predicted by LEWICE 3.0 is closer to the experimental data, but this is because the ice density correlation was determined from these results. More cases are needed to determine if this result is real or a by-product of the correlation. More comparisons, including glaze ice shapes, are needed to fully assess the splashing model.

**Figure 26: Ice Mass Comparison for Example Cases**

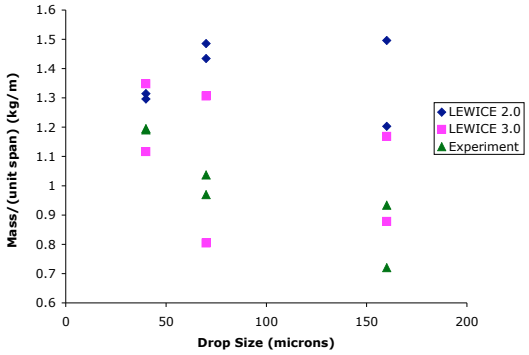


## Conclusions

A review of the physical effects of large droplet phenomena confirmed that droplet splashing is the primary physics that is not modeled in icing software. Several other phenomena such as drop breakup, drop-drop interactions and changes in drag, lift and ice density were also covered. Empirical models for these phenomena were presented. The resulting effect on water collection, ice shape and ice mass for LEWICE were presented.

The results show that the current empirical splashing models could only account for splashing effects near the leading edge. The models, all of which are based on the velocity component normal to the surface, could not explain the measured decrease in water collection near the impingement limits. However, it was necessary to extrapolate values from the empirical data for this effort. It is hypothesized that droplets that impact at high total velocities (> 30 m/s) but low impact angles (< 20°) may rebound in a manner different than the current experimental data at the lower velocities.

Ice shape profiles show similar results to previous LEWICE outputs since an ice density correlation was added to counteract the loss in mass due to splashing. The ice mass results for the current model are closer to the experimentally measured values, but the same dataset that was used to generate the correlation was used to assess the results.

## Acknowledgements

The authors would like to acknowledge Colin Bidwell and Dean Miller from the NASA Glenn Icing Branch as well as Paul Tsao and David Anderson from the Ohio Aerospace Institute for their insight and experience with SLD issues. The first author would also like to acknowledge the continued financial support from NASA Glenn for this research.

## References

1. Wright, W.B., and Potapczuk, M. G., "Computational Simulation of Large Droplet Icing," Proceedings of the FAA International Conference on Aircraft Inflight Icing, pp. 545-55, Aug. 1996.

2. "In-flight Icing Encounter and Loss of Control Simmons Airlines, d.b.a. American Eagle Flight 4184 Avions de Transport Regional (ATR) Model 72-212, N401AM, Roselawn, Indiana October 31, 1994", NTSB Report Number: AAR-96-01

3. Wright, W. B., "Users Manual for the NASA Glenn Ice Accretion Code LEWICE Version 2.2.2," NASA CR 211793, Aug. 2002.

4. Clift, R., Grace, J. R., and Weber, M. E., "Bubbles, Drops, and Particles," Academic Press, New York, 1978.

5. Tavlarides, L. T., Coulalogou, C. A., Zeitlin, M. A., Klinzing, G. E., Gal-or, B., "Bubble and Drop Phenomena," Ind. And Eng. Chem. V. 62, no. 11, pp. 6-27, Nov. 1970.

6. Michaelides, E. E., "Review – The Transient Equation of Motion for Particles, Bubbles, and Droplets," J. Fluids Engr., v. 119, pp. 233-246, June 1997.

7. Saffman, P. G., "The Lift on a Small Sphere in a Slow Shear Flow," J. Fl. Mech, v. 22, No. 2, pp. 385-400, 1965.

8. Mashayek, F. "Droplet Turbulence Interactions in Low-Mach-number Homogeneous Shear Two-Phase Flows," J. Fl. Mech., v. 367, pp. 163-202, 1998.

9. Marchioli, C. and Soldati, A., "Mechanism for Particle Transfer and Segregation in a Turbulent Boundary Layer," J. Fl. Mech., v. 468, pp. 283-315, 2002.

10. Shin, M., Kim D. S., Lee, J. W., "Deposition of Inertia-Dominated Particles Inside a Turbulent Boundary Layer," Int. J. of Multiphase Flow, v. 29, pp. 893-926, 2003.

11. Bhargava, C., Loth, E., and Potapczuk, M.,"Simulation of Droplet Distributions in the NASA Glenn Icing Research Tunnel, AIAA 04-0563, Jan. 2004.

12. Papadakis, M., Elangonan, R., Freund, Jr., G. A., Breer, M., Zumwalt, G. W. and Whitmer, L., "An Experimental Method for Measuring Water Droplet Impingement Efficiency on Two- and Three-Dimensional Bodies," NASA CR 4257, Nov. 1989.

13. Beard, K. V., and Pruppacher, H. R., "A Determination of the Terminal Velocity and Drag of Small Water Drops by Means of a Wind Tunnel," J. Atmos. Sci, v. 26, pp. 1066-1072, 1969.

14. Mulholland, J. A., Srivastava, R. K., Wendt, J. O. L., "Influence of Droplet Spacing on Drag Coefficient in Nonevaporating, Monodisperse Streams, v. 26, No. 10, pp. 1231-7, Oct. 1988.

15. Syrnaios, D. S., Pelekasis, N. A., and Tsamopoulos, J. A., "Boundary Layer Flow of Air Past Solid Surfaces in the Presence of Rainfall," J. Fl. Mech., v. 425, pp. 79-110, 2000.

16. Krzeczkowski, S. A., "Measurement of Liquid Droplet Disintegration Mechanism," int. J. Multiphase Flow, v. 6, pp. 227-239, 1980.

17. Hsiang, L. P. and Faeth. G. M., "Secondary Drop Breakup in the Deformation Regime," AIAA 92-0110, Jan. 1992.

18. Ibrahim, E. A., Yang, H. Q., and Przekwas, A. J., "Modeling of Spray Droplets Deformation and Breakup," J. Prop., v. 9, No. 4, pp. 651-654, 1993.

19. Dai, Z. and Faeth, G. M., "Temporal Properties of Multimode Secondary Droplet Breakup," AIAA 99-0333, Jan. 1999.

20. Ice Protection Harmonization Working Group, "Appendix X (Draft)", 2003.

21. Potapczuk, M. G., "Ice Mass Measurements: Implications for the Ice Accretion Process," AIAA 2003-387, Jan. 2003.

22. Stow, C. D., and Hadfield, M. G., "An Experimental Investigation of Fluid Flow Resulting from the Impact of a Water Drop with an Unyielding Dry Surface," Proc. R. soc. Lond. A v. 373, pp. 419-441, 1981.

23. Macklin, W. C. and Metaxas, G. J., "Splashing of Drops on Liquid Layers," J. App. Phys., v. 47, No. 9, pp. 3963-3970, Sept. 1976.

24. Jayarante, O. W. and Mason, B. J., "The Coalescence and Bouncing of Water Drops at an Air/Water Interface," proc. Roy. Sci. A., v. 280, pp. 545-565, 1965.

25. Wright, A. C., "A Physically-Based Model of the Dispersion of Splash Droplets Ejected from a Water Drop Impact," Earth Surf. Proc. And Landforms, v. 11, pp. 351-367, 1986.

26. Harlow F. H. and Shannon, J, P., "The Splash of a Liquid Drop," J. App. Phys., v. 38, No. 10, pp. 3855-3866, 1967.

27. Yarin. A. L. and Weiss, D. A., "Impact of Drops on Solid Surfaces: Self-Similar Capillary Waves, and Splashing as a New Type of Kinematic Discontinuity," J. Fluid Mech., v. 283, pp. 141-173, 1995.

28. Weiss D. A., "Periodischer Aufprall monodisperser Tropen gleicher Geschwindigkeit auf feste Oberflächen," Mitteilungeen aus dem Max-Plank-Institut für Stromungsforschung, Gottingen, Nr. 112, 1993.

29. Rein, M., "Phenomena of Liquid Drop Impact on Solid and Liquid Surfaces," Fl. Dyn. Res., v. 12, pp. 61-93, 1993.

30. Chandra, S. and Avedisian, C. T., "On the Collision of a Droplet with a Solid Surface," Proc. Roy. Soc. Lond. A, v. 432, pp. 13-41, 1991.

31. Hirt, C. W., Nicholls, B. D., "Volume of Fluid Method for Dynamic Free Boundary," J. Comp. Phys., v.39, 1981.

32. Trapaga, G. and Szekely, J., "Mathematical Modeling of the Isothermal Impingement of Liquid Drops in the Spraying Process," Metallurgical Transactions B, v. 22B, pp. 901-914, Dec. 1991.

33. Tan, S. C. and Papadakis, M., " General Effects of Large Droplet Dynamics on Ice

Accretion Modeling," AIAA 2003-392, Jan. 2003.

34. Mundo, C., Sommerfeld, M., and Tropea, C., "Droplet-Wall Collisions: Experimental Studies of the Deformation and Breakup Process," Int. J. Multiphase Flow, v. 21, No. 2, pp. 151-173, 1995.

35. Mundo, C., Tropea, C. and Sommerfeld, M., "Numerical and Experimental Investigation of Spray Characteristics in the Vicinity of a Rigid Wall," Exp. Thermal and Fl. Sci., v. 15, pp. 228-237, 1997.

36. Mundo, C., Sommerfeld, M., and Tropea, C., "On the Modeling of Liquid Sprays Impinging on Surfaces," Atomization and Sprays, v. 8, pp. 625-652, 1998.

37. Feo, A., Personal Communication, Dec. 2003.

38. Lee, S. H. and Ryou, H. S., "Development of a New Model and Heat Transfer Analysis of Impinging Diesel Sprays on a Wall," Atomization and Sprays, v. 11, pp. 85-105, 2001.

39. Cossali, G. E., Brunello, G., Coghe, A., and Marengo, M., "Impact of a Single Drop on a Liquid Film: Experimental Analysis and Comparison with Empirical Models," Italian Conf. on Thermofluid Dyn., July, 1999

40. Stanton, D. W. and Rutland, C.J., "Multi-Dimensional Modeling of Heat and Mass Transfer of Fuel Films Resulting from Impinging Sprays," Soc. Auto. Eng. 960628, 1998.

41. Marengo, M. and Tropea, C., "Zwischenbericht zum Forschungsvorhaben Aufprall von Tropfen auf Flusssigkeitsfilme," Tr 194/10 1,2, Deutsche Forschungsgemainschaft, Apr. 1999.

42. Trujillo, M. F., Matthews, W.S., Lee, C.F., and Peters, J.E., "Modeling and Experiment of Impingement and Atomization of a Liquid Spray on a Wall," Int. J. Engine Research, v. 1, No. 1, pp. 87-104, 2000.

43. Schmehl, R., H. Rosskamp, M. Willmann, Wittig, S., "CFD Analysis of Spray Propagation and Evaporation Including Wall Film Formation and Spray/Film Interactions," Gas turbine Eng. Comb., Emissions and Fuels, pp. 1-11, June 1999.

44. Samenfink, W., Elsaber, A., Dullenkopf, K., and Wittig, S., "Droplet interaction with Shear-Driven Liquid Films: Analysis of Deposition and Secondary Droplet Characteristics," Int. J. of Heat and Fluid Flow, v. 20, pp. 462-9, 1999.

45. Rutkowski, A., Wright, W. B. and Potapczuk, M. G., "Numerical Study of Droplet Splashing and Re-Impingement," AIAA 2003-388, Jan. 2003.

46. Papadakis, M., Hung, K. E., Vu, G .T., Yeong, H. W., Bidwell, C. S., Breer, M. D., Bencic, T. J., "Experimental Investigaion of Water Droplet Impingement on Airfoils, Finite Wings, and an S-Duct Engine Inlet, NASA TM 2002-211700, Oct. 2002.